Journal of Atmospheric and Solar-Terrestrial Physics 72 (2010) 1241–1250

Contents lists available at ScienceDirect

Journal of Atmospheric and Solar-Terrestrial Physics

journal homepage: www.elsevier.com/locate/jastp

Spatial distribution of near-surface CO over bay of Bengal during winter: role of transport

Girach Imran Asatar, Prabha R Nair*

Space Physics Laboratory, Vikram Sarabhai Space Centre, Trivandrum 695 022, India

ARTICLE INFO

Article history:
Received 5 February 2010
Received in revised form
24 July 2010
Accepted 26 July 2010
Available online 12 August 2010

Keywords:
Carbon monoxide in the atmosphere
Troposphere: constituent transport and chemistry
Anthropogenic effects
Pollution: urban and regional

ABSTRACT

As part of Integrated Campaign for Aerosols, gases and Radiation Budget (ICARB), cruise-based measurements of near-surface CO were carried out over Bay of Bengal (BoB) covering the latitude–longitude sector 3.5°N–21.0°N and 76.0°E–98.0°E, during winter months of December 2008 to January 2009. These in-situ measured CO mixing ratio varied in the range of 80–480 ppbv over this marine environment with the distinct spatial pattern. The highest mixing ratios were measured over southeast-BoB with mean value of 379 ± 58 ppbv. CO mixing ratios were high over north-BoB compared to southern BoB. These in-situ measurements were compared with the satellite-measured surface CO obtained from Measurements of Pollution in the Troposphere (MOPITT) onboard TERRA and found to be in good agreement over most of the regions, except at southeast-BoB. Surface CO and column CO from MOPITT data showed a similar spatial pattern. Based on the analysis of airmass back-trajectories, satellite-based spatial map of CO distribution over Asian region and Potential Source Contribution Function analysis, different pathways of transport of CO were identified. Transport from northern landmass as well as from south-east Asia has a significant influence in the spatial variation of CO over BoB. Winter-time mixing ratio of CO was found to be higher compared to those measured during other campaigns conducted during February–March 1999, 2001 (pre-monsoon) and September–October, 2002 (post-monsoon).

© 2010 Elsevier Ltd. All rights reserved.

1. Introduction

The role of carbon monoxide (CO) in diminishing the OH-based oxidizing capacity of the troposphere is well established (Logan et al., 1981; Thompson, 1992). CO can also elevate the concentrations of greenhouse gases like methane and tropospheric ozone through its reactions with OH radical, and hence indirectly contribute to global warming (Brühl and Crutzen, 1999). In addition to this, CO is recognized as an environmental pollutant with adverse effect on health. It is also used as a tracer to study transport of global and regional pollutants from industrial activities and large-scale biomass burning. CO has both natural and anthropogenic sources. It is an outcome of natural tropical forest fires, human initiated forest fires mostly for agricultural activities (Crutzen and Andreae, 1990), firewood/agricultural waste burning, fossil fuel combustion and oxidation of biogenic hydrocarbon from plants. Besides these sources, ocean is known to be a natural source of CO. Sunlight initiated photolysis of chromophoric dissolved organic matter is one of the dominant sources of CO in the open ocean (Ohta, 1997; Stubbins et al., 2006). Production of CO is more at coastal waters than the open ocean (Jones and Amador, 1993). The net contribution of global oceans to atmospheric CO is about 1000 ± 200 Tg per year, which represents the largest single natural source of atmospheric CO (Zuo et al., 1998). Oceanic sources of CO contribute to ~5% of that produced through burning of fossil fuel (Swinnerton et al., 1970; Stubbins et al., 2006). The background mixing ratios of CO over oceans include the continental emission in the same latitudinal band also. However, the effect of oceanic source could not be addressed in the present study, because the detection limit of the instrument is 50 ppbv.

As a consequence of the increasing population, urbanization and industrial growth, atmospheric load of CO and several other pollutants has increased over decades. Surface CO measurements over the globe through the Cooperative Air Sampling Network of Climate Monitoring and Diagnostic Laboratory of the National Oceanic and Atmospheric Administration (NOAA/CMDL) (Novelli et al., 1992), satellite observations (Liu et al., 2006) and short-duration campaigns (Mühle et al., 2002; Lal et al., 2006; Sahu et al., 2006; Li et al., 2007) indicated that CO is highly variable both temporally and spatially. In Northern hemisphere, the rate of CO concentration increase is found to be ~1–2% per year (Khalil and Rasmussen, 1988; Dianov-Klokov and Yurganov, 1989; Zander et al., 1989) during 1950–1985. Later, during 1988–1992

* Corresponding author. Tel.: +91 0471 2562563; fax: +91 0471 2706535.
E-mail address: prabha_nair@vssc.gov.in (P.R. Nair).

1364-6826/$ - see front matter © 2010 Elsevier Ltd. All rights reserved.
doi:10.1016/j.jastp.2010.07.025

period, six different sites representing polar, middle and tropical latitudes of both the hemispheres (Pt. Barrow, Alaska; Cape Meares, Oregon; Cape Kumukahi and Mauna Loa Observatory, Hawaii; Cape Matatula, Samoa; Cape Grim, Tasmania; Palmer Station and South Pole, Antarctica) showed a decrease in CO concentration at the rate of $-2.6 \pm 0.8\%$ per year (Khalil and Rasmussen, 1994). An increase of 0.96 ppbv/year has been reported over Russian region from 1970 to 1999 (Grechko et al., 2000). Owing to the control measures taken, several nations, including United States, Canada and many European countries, succeeded in cutting down the CO emissions complying with their air quality standards (http://www.epa.gov/airtrends/carbon.html; Eisinger et al., 2002; http://environment.alberta.ca/01644.html). Through the analysis of flask, air samples collected from a network of stations spread all over the globe, Steele et al. (2003) have reported that many of these stations do not show any long term trends in CO during the period from 1984 to 2001. However, some anomalous increase was observed on global scale during 1997–1998 (Langenfelds et al., 2002). The model-estimated global-averaged concentration of CO is 27 ppbv before 1840 and 76 ppbv in 1991 (Zhang et al., 2001). CO measurement by 'Measurements Of Pollution In The Troposphere' (MOPITT) on-board TERRA is a potential tool in identifying the emission sources of CO with the global coverage. It has been used effectively to study CO plumes from forest fires (Liu et al., 2005), intercontinental transport of pollution (Edwards et al., 2003, 2006; Heald et al., 2003) and convective transport of pollution to the upper troposphere (Kar et al., 2004, 2006; Li et al., 2005; Liu et al., 2005). In spite of all these, direct/in-situ measurements of CO are still insufficient for understanding the global distribution of CO in space and time. This is particularly true for Asian region, where long-term measurements with sufficient spatial resolution is lacking and very few campaign mode studies are available like East Asian Study of Tropospheric Aerosols: an International Regional Experiment (EAST-AIRE), Indian Ocean Experiment (INDOEX), Bay of Bengal Experiment (BOBEX), Bay of Bengal Processes Studies (BOBPS), etc. with limited spatial and temporal resolution (Li et al., 2007; Mühle et al., 2002; Lal et al., 2006; Sahu et al., 2006).

The 'Integrated Campaign for Aerosols, gases and Radiation Budget (ICARB)' conceived under the Geosphere Biosphere Programme of Indian Space Research Organization (ISRO-GBP) has the major objective of mapping aerosols and trace gases over Bay of Bengal (BoB), identifying transport mechanisms and studying their impacts on regional radiative forcing. The second phase of ICARB also called as W_ICARB was conducted during the winter period of December 27, 2008 to January 30, 2009. For the first time, ship-based measurements were carried out with vast longitudinal coverage over BoB, including southern and eastern parts of this oceanic region. During this period of study (northern winter), the synoptic wind was northeasterly (Asnani, 1993) favouring an outflow of continental airmass over to BoB and Indian Ocean region. This along with the important geographical feature of BoB surrounded by landmass on three sides is conducive for accumulation of aerosols and trace gases in this marine environment. The present study focused on the spatial variation of near-surface CO over the entire BoB. While the earlier studies were conducted during the late winter period (February–March), or post-monsoon months of September–October, the present study was conducted in December–January to bring out the winter-time spatial features for the first time. The in-situ measured data was compared with the satellite-based measurement of surface CO from MOPITT. The spatial pattern of CO was examined in the light of airflow patterns, airmass back-trajectories, Potential Source Contribution Function (PSCF) analysis and satellite-based maps of CO distribution to identify the transport pathways.

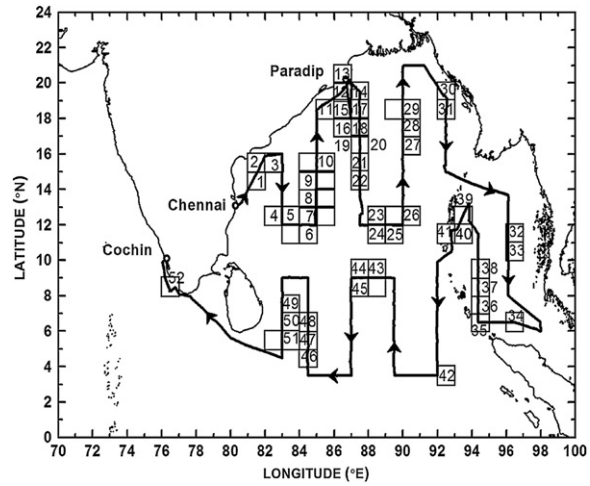

Fig. 1. Cruise track of SK 254 over the Bay of Bengal during W_ICARB. The numbers shown in the boxes are the grid numbers, which is assigned for the comparison with MOPITT retrievals.

2. Cruise track

Fig. 1 shows the track (thick solid line) of the Oceanic Research Vessel *Sagar Kanya* during the present cruise (No. SK 254). Other details of Fig. 1 are further explained in section 5.2. Ship started sailing from Chennai (13.1°N, 80.3°E) on December 27, 2008 moving towards north-east. The arrows in the figure show the direction of movement of the ship. It had several longitudinal and latitudinal scans over BoB covering latitude sector 3.5–21.0°N and longitude sector 76.0–98.0°E. Except for the three short stoppages of 13–15 h duration, the ship was sailing continuously. The cruise ended on 30 January 2009 at Cochin (10.1°N, 76.3°E), completing 34 days of a voyage. The cruise did not encounter any severe weather system during the campaign.

3. Meteorological conditions over cruise region

Fig. 2a–c shows the mean synoptic wind flow pattern at 925 hPa, rms (root mean square) wind-speed and the maximum wind-speed, respectively, over BoB region, for the cruise period, as obtained from NCEP/NCAR reanalysis (http://www.esrl.noaa.gov/psd). While the length of an arrow is proportional to wind-speed, arrowhead indicates direction (the colour also indicates the wind-speed). The flow patterns reveal that over north/head-BoB (north of ~16°N latitude) winds are northerlies with relatively low wind-speed. South of ~16°N latitude, winds are strong and north-easterlies. Fig. 2b and c confirms that the low wind-speed regions are not the result of stronger wind in opposite directions. Continuous on-board measurements of meteorological parameters viz., temperature (*T*), relative humidity (*RH*), pressure (*P*), wind-speed (*WS*) and wind direction (*WD*) were also carried out using an automatic weather station (NRG Systems, USA) mounted on the boom of the ship. A GPS receiver onboard provided the coordinates of the ship. The wind measurements were corrected for ship speed and direction. Over the cruise region, air temperature ranged between 22 and 29 °C (with higher values over southern BoB) and RH between 50% and 98%. Wind showed large variation over the region from calm conditions over north-BoB to wind-speed as high as ~12 m/s over the southern region. On-board winds were mostly northerlies/north-easterlies. More detailed discussions on meteorological conditions are given in Section 5.1 along with Figs. 4 and 5.

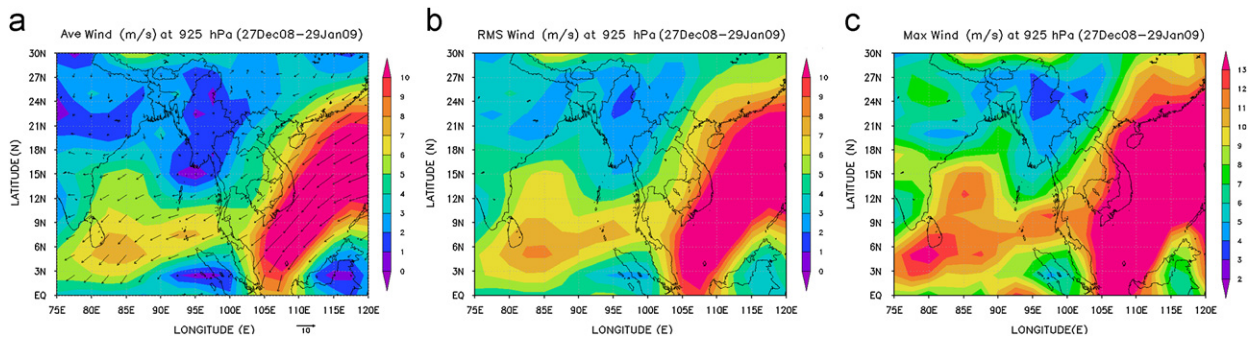

Fig. 2. (a) Mean airflow pattern, (b) rms (root mean square) wind and (c) maximum wind at 925 hPa over BoB during cruise period. The colour and the arrow length show wind-speed and arrow head shows the wind direction.

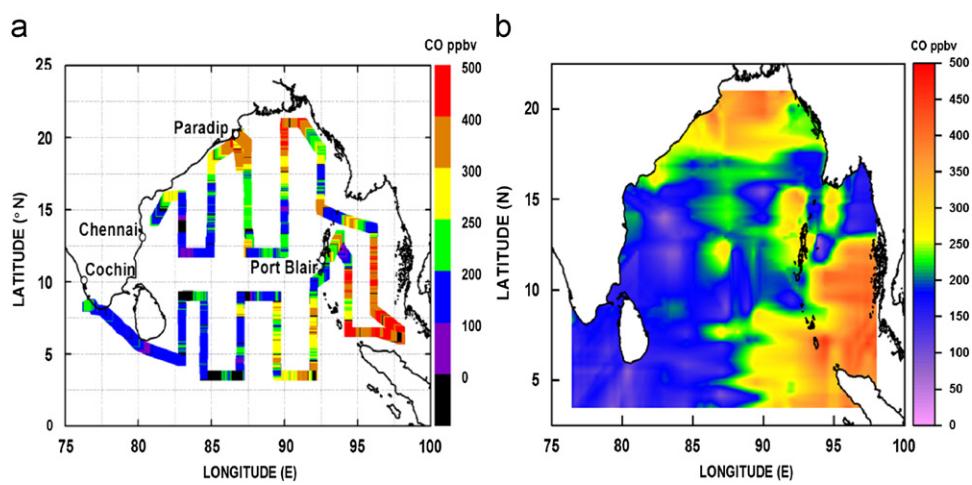

Fig. 3. (a) Variation of CO mixing ratio along the cruise track over BoB and (b) surface map of CO mixing ratio over BoB obtained by using interpolation.

4. Instrumentation and data

Carbon monoxide (CO) measurements were carried out along the cruise track by using an online gas filter correlation CO analyzer (Model CO12 Module) from Environnement S.A., France. The analyzer works on the principle of infrared absorption of CO at the wavelength of 4.67 μm. The optical filter combined with a gas filter called 'correlation wheel,' gives highly selective measurement of CO gas by eliminating interference from any gas with absorption peak close to that of CO. The analyzer is capable of measuring CO in the range 0.05–200 ppm (with auto-ranging facility). The instrument has lower detection limit of 50 ppbv, linearity 1% and response time of 40 s. It was calibrated onboard periodically using CO standard diluted with custom-made calibrator, upto the concentration of 1.1 ppm. The inlet was kept on port side at a height of approximately 10 m from sea-surface. Data was recorded at an interval of 5 min. Extra care is taken to avoid any exhaust from ship, by continuously monitoring wind direction.

In addition to the in-situ measured CO data, satellite-based surface CO obtained from MOPITT was also used in this study. MOPITT measures upwelling IR radiation at 4.7 μm and CO mixing ratio is retrieved, using gas correlation radiometry. Level-3 MOPITT data of surface CO and column CO were obtained from the website https://wist.echo.nasa.gov/api/and/or http://eosweb.larc.nasa.gov/. This data is available on daily/monthly basis with the grid size of 1° latitude × 1° longitude, and for day and night separately. Night is defined when the solar zenith angle is greater than 80°. The retrieval sensitivity of MOPITT is greater for daytime overpass than for nighttime overpass (http://shire.larc.nasa.gov/PRODOCS/mopitt/Quality_Summaries/mopitt_level3_ver4.html). The surface CO obtained through retrieval algorithm Version 4 (V4) has been compared with that obtained though Version 3 (V3).

5. Results and discussion

5.1. Spatial variation of CO over BoB

Mixing ratio of CO, measured over the cruise track, is presented in Fig. 3a by coloured squares marked on the track along with the colour scale shown by the side. The black squares on the cruise track denote the absence of data. Based on the data shown in Fig. 5a, surface plot has been generated and given in Fig. 3b, which depicts the spatial variation of CO over this marine environment. Very few measurements (~0.8% of total measurements), in which CO mixing ratios were below the lower detection limit of the instrument, are discarded in this study. Figs. 3a and 3b clearly show the heterogeneity in the distribution of CO over BoB. There exist certain hotspots in the spatial distribution of near-surface CO over the cruise region. Relatively high CO mixing ratio (140–460 ppbv) was observed over head-BoB (north of ~16°N), including the coastal regions with the mean value ± standard deviation being 290 ± 72 ppbv. Consistently, highest mixing ratio of 379 ± 58 ppbv was observed over the southeast-BoB (south of ~11°N, east of ~94°E) and near to Andaman islands. Relatively low values of CO (with a mean value of 167 ± 39 ppbv) lying in the range 80–300 ppbv were measured in the southwest-BoB (south of ~16°N, west of ~87°E).

It is known that meteorological conditions can influence the production, destruction and transport of CO (Klonecki and Levy, 1997). Fig. 4a–f shows the day to day variation of *RH*, *T*, *P*, *WD* and *WS* along with corresponding CO mixing ratios as measured onboard the ship and along the cruise track. A close examination of these figures reveals that CO mixing ratio has not strongly influenced any of these meteorological parameters, except that it shows a positive correlation with RH during the initial phase of the cruise (till January 17). From January 18 onwards (when it was traversing south BoB), the ship encountered a region of low pressure and higher temperature, where the CO mixing ratios were low. The dependence of CO and RH stated above is further examined by grouping the CO data in terms of RH and averaging for RH intervals of 5%. Fig. 5 shows a scatter plot between mean RH and CO mixing ratios with the solid line representing the best-fit line (correlation coefficient ~0.96). RH level is indicative of water vapor – a source of OH radical – which is considered as a sink for CO as well as CH_4. However, several recent studies indicate that, in the atmosphere, one of the major sources CO is an oxidation of methane by OH (Holloway et al., 2000; Wang and Prinn, 1999). Also oceans are known to be sources of methane and many other hydrocarbons, even though they are not well quantified. It is estimated that while production of CO from methane oxidation represents 53% of this chemical production, the oxidation of isoprene, terpenes and other hydrocarbons represents 20%, 4% and 23%, respectively, of it (Granier et al., 2000). Hence the positive correlation between RH and CO could be partly due to oxidation of CH_4 and subsequent CO production. Lal et al. (2006) have reported significant concentration of CH_4 over the BoB region. However, in the absence of simultaneous measurements of CH_4 and other hydrocarbons, it is not possible to quantify this contribution, and hence needs further studies.

Fig. 6 clearly depicts longitudinal variations in the mixing ratio of CO with an increase towards eastern longitudes. However, these variations are latitude dependent. Hence region/latitude dependent longitudinal gradients were estimated. Based on the latitude, the entire data were grouped into three sectors as: (1) head-BoB (latitude sector 16°N–21°N), (2) mid BoB (12°N–16°N) and (3) southern BoB (3.5°N–12°N). The scatter plots in Fig. 6a–c show the longitudinal variation of the mixing ratio of CO in these three latitude sectors. At the head-BoB region, CO mixing ratio is high and more or less steady with no significant variation with longitude. However, if the last point in Fig. 6a is removed, the linear gradient will be improved (correlation coefficient of 0.83). But there is no reason to ignore this point, since it is the mean of ~266 measurements (5 min interval). The low

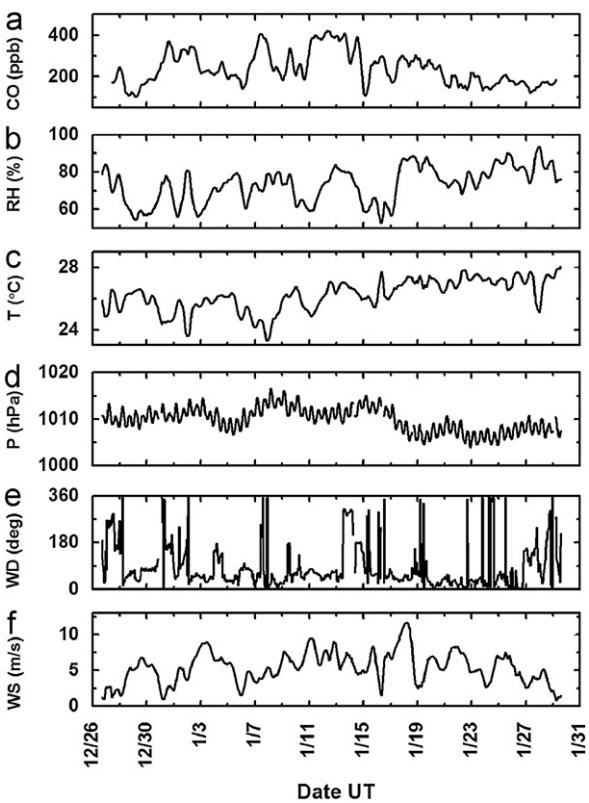

Fig. 4. Mean (a), CO (b), RH (c), temperature (d), pressure (e), wind direction and (f) wind-speed along the cruise track, averaged on hourly basis.

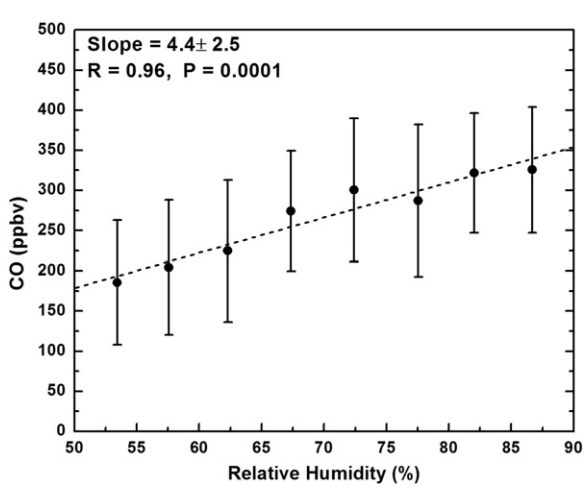

Fig. 5. Variation of averaged CO mixing ratio with relative humidity.

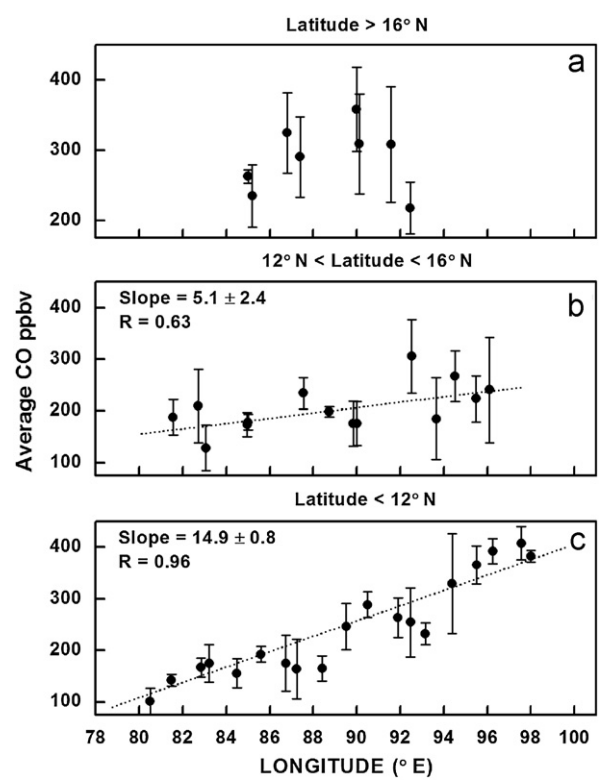

Fig. 6. Longitudinal gradient for latitude region: (a) above 16°N, (b) between 12° and 16°N and (c) below 12°N.

wind-speed (~1–6 m/s) in this region was also unfavourable for dispersion. In addition, relatively low temperature over head-BoB (Fig. 4c) reduces the effectiveness of vertical mixing. Towards south, CO mixing ratio exhibits longitudinal gradient with an increasing trend towards eastern longitudes. The magnitude of the linear gradient which is 5.1 ± 2.4 ppbv (with correlation coefficient $R=0.63$) in latitude sector 12°–16°N which increases to 14.9 ± 0.8 ppb/°longitude (with correlation coefficient $R=0.96$) at latitudes south of 12°N. The large longitudinal gradients in southern BoB could be partly due to the stronger winds (~6–8 m/s) prevailed there, as seen in Fig. 2a. Such strong winds prevailing for a longer period facilitate transport to longer distances within short time interval, leading to the large spatial gradient. As over head-BoB, the air parcel travels over the marine environment where no major sources are active and deposition/dispersion is possible. On the other hand, weak winds enable stagnation and confinement resulting in weak spatial gradients. The observed spatial pattern was examined in detail in the light of airflow patterns and airmass back-trajectories and the results are presented in section 5.3.

5.2. Comparison of in-situ measurements of surface CO with MOPITT retrievals

MOPITT measurements are widely used for obtaining global picture of the CO distribution. Kar et al. (2008) has effectively used MOPITT data for identifying the emission sources over Indian subcontinent, providing an evidence for the sensitivity of MOPITT in the lower troposphere. In the present study, the cruise-based in-situ data of near-surface CO over BoB were compared with the Level-3 data of MOPITT retrieved, using the algorithms V3 and V4. For comparison of insitu measured and MOPITT-retrieved CO data on daily basis, spatial grids were so chosen that the cruise track passed through any part of the grid. Grids were numbered sequentially from starting point of the cruise to the end. The insitu measured data falling in each grid was averaged for day and night separately and compared with corresponding MOPITT data. When cruise track passes through the edge of the grid, the adjacent grid (if available) was also considered for the comparison. The grid numbers written outside the grid (e.g. 19 and 20) denote that the respective grid points correspond to two days. The latitude and longitude corresponding to each grid along with the date of measurement are listed in Table 1 for identifying the location. Fig. 7 shows a comparison of in-situ measured CO and corresponding MOPITT-measured surface values for the same period and same location. The grid numbers are shown on the X-axis. Hollow/solid circles and triangles represent daytime and nighttime measurements, respectively, (http://shire.larc.nasa.gov/PRODOCS/mopitt/Quality_Summaries/). Error bars denote the standard deviation (for all day/night measurement points which fall within the grid) for in-situ measured CO and uncertainty in

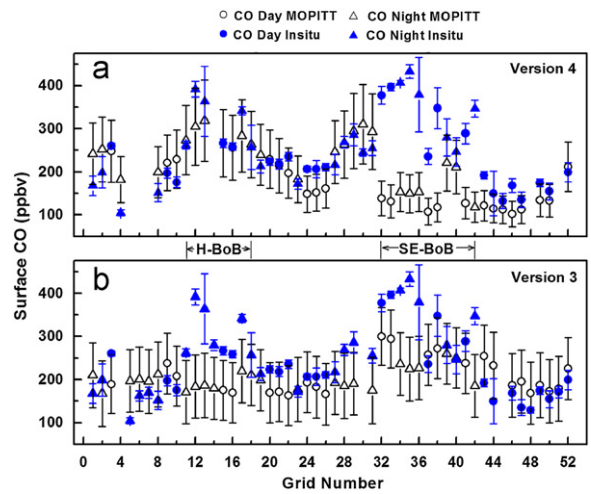

Fig. 7. Comparison between in-situ measured surface CO and MOPITT-retrieved surface CO obtained, using retrieval algorithms: (a) Version 4 and (b) Version 3. Hollow circles and triangles represent daytime and nighttime measurements, respectively, of MOPITT, whereas solid circles and triangles represent daytime and nighttime, respectively, of insitu measurements.

Table 1
The grid numbers in Fig. 6 in terms of the location (latitude and longitude grid) and date.

Grid no.	Date	Latitude (°N)	Longitude (°E)	Grid no.	Date	Latitude (°N)	Longitude (°E)
1	12/27/2008	14.5	81.5	27	1/6/2009	16.5	90.5
2	12/27/2008	15.5	81.5	28	1/6/2009	17.5	90.5
3	12/28/2008	15.5	82.5	29	1/6/2009	18.5	90.5
4	12/29/2008	12.5	82.5	30	1/8/2009	19.5	92.5
5	12/29/2008	12.5	83.5	31	1/8/2009	18.5	92.5
6	12/29/2008	11.5	84.5	32	1/11/2009	11.5	96.5
7	12/29/2008	12.5	84.5	33	1/11/2009	10.5	96.5
8	12/29/2008	13.5	84.5	34	1/13/2009	6.5	96.5
9	12/30/2008	14.5	84.5	35	1/13/2009	6.5	94.5
10	12/30/2008	15.5	85.5	36	1/13/2009	7.5	94.5
11	12/31/2008	18.5	85.5	37	1/14/2009	8.5	94.5
12	12/31/2008	19.5	86.5	38	1/14/2009	9.5	94.5
13	12/31/2008	20.5	86.5	39	1/15/2009	12.5	93.5
14	12/31/2008	19.5	87.5	40	1/15/2009	11.5	93.5
15	1/1/2009	18.5	86.5	41	1/16/2009	11.5	92.5
16	1/1/2009	17.5	86.5	42	1/18/2009	3.5	92.5
17	1/2/2009	18.5	87.5	43	1/21/2009	9.5	88.5
18	1/2/2009	17.5	87.5	44	1/21/2009	9.5	87.5
19	1/2/2009	16.5	87.5	45	1/21/2009	8.5	87.5
20	1/3/2009	16.5	87.5	46	1/24/2009	4.5	84.5
21	1/3/2009	15.5	87.5	47	1/24/2009	5.5	84.5
22	1/3/2009	14.5	87.5	48	1/24/2009	6.5	84.5
23	1/4/2009	12.5	88.5	49	1/26/2009	7.5	83.5
24	1/5/2009	12.5	88.5	50	1/26/2009	6.5	83.5
25	1/5/2009	11.5	89.5	51	1/26/2009	5.5	83.5
26	1/5/2009	12.5	90.5	52	1/29/2009	8.5	76.5

the case of MOPITT data retrieval. From Fig. 7a, it can be seen that both the measurements are in good agreement, except at few locations over the south-east BoB (Grid nos. 32–42), where CO mixing ratios are relatively high (approximately >350 ppbv). However, the high CO values in the region of head-BoB (Grid nos. 11–18) are in good agreement. Fig. 7b gives a comparison of in-situ measurements with surface CO at 1000 hPa obtained from MOPITT, using the retrieval algorithm V3. In this case, the satellite-retrieved values deviate from the in-situ measured values and are generally underestimated when the mixing ratio >250 ppbv. However, over south-east BoB (Grid nos. 32–42), where in-situ values showed large deviation from satellite measured values retrieved using V4, those obtained by using V3 were closer to in-situ measurements.

Fig. 8 shows the scatter plot between the in-situ measured CO mixing ratio and the MOPPITT retrieved (V4) near-surface CO, which illustrates the good agreement between the two. The points shown by hollow circles represent those measured over southeast-BoB region. The straight line represents the best-fit line obtained through linear regression method (note that the open circles are not included in estimating this fit). It has a slope of 0.77 ± 0.11 and the y-intercept of 44 ± 25 with correlation coefficient of 0.77 with the significance level of $P < 0.0001$ (Fisher, 1970). If the open circles are also included, correlation coefficient drops to 0.15.

The most probable causes for the discrepancy in in-situ measured and satellite-retrieved CO values using V4, as shown by the hollow circles in Fig. 8, (which represent the southeast-BoB) could be the inadequacies in (1) accounting water vapor effect, (2) removal of cloud effects, (3) apriori information of CO used in the retrieval algorithm and (4) noise removal. CO retrieval using V4 incorporates a corrective algorithm for accounting water vapor effects (MOPITT Validated Version 4 Product User's Guide). Moreover RH values and columnar water vapor content (measured using Microtops-II) do not show significant changes during the period. Thus, effects of water vapor on the retrieved data may be ruled out. Prior to retrieval, data is checked for cloudy or clear conditions based on both MOPITT radiances themselves and a "cloud mask" produced from near-simultaneous observations by Terra/MODIS ("MODerate resolution Imaging Spectroradiometer") instrument. The cloud detection module ("MOPCLD") is same for V4 and V3. Furthermore, an improved noise removal

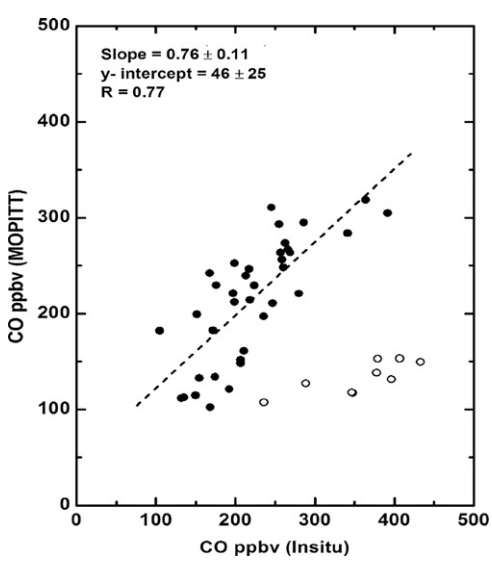

Fig. 8. Scatter plot between in-situ measurement of surface-CO and that retrieved from MOPPITT. The hollow circles represent the measurements over southeast-BoB and not included in the line fitting.

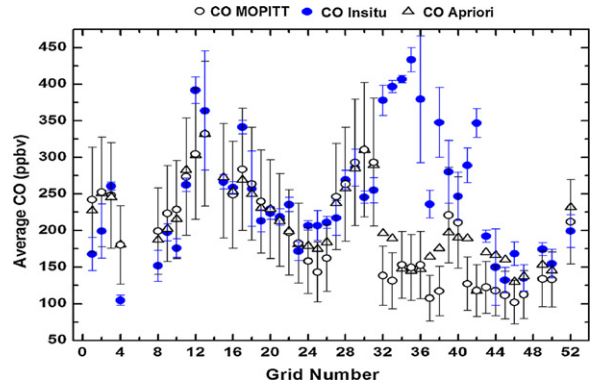

Fig. 9. Comparison between MOPITT-retrieved surface CO and apriori CO obtained from MOPITT level-3 V4. Insitu-measured CO values are also shown here.

technique is used in V4 compared to V3, which increases the accuracy of the retrieved data. Another important factor is the apriori information used in retrieval algorithm V4, which is different from V3. Fig. 9 shows the comparison of CO mixing ratios (MOPITT and insitu) along with the apriori information used in the retrieval algorithm V4 as obtained from the respective MOPITT data file. It can be clearly seen that when the apriori values are close to actual mixing ratios, MOPITT retrievals and insitu measurements match well. But when the apriori values deviate significantly from actual mixing ratios (Grid nos. 32–42 in Fig. 8), MOPITT retrieved data also shows large variations from the insitu-measured values. Thus, the observed discrepancy could be partly due to the inadequacy of apriori information.

5.3. Transport pathways of CO over to BoB

With a view to investigate the pathways of transport of CO over to BoB, the spatial maps of surface CO and column CO over Asian region were obtained from level-3 data of MOPITT (V4). Fig. 10a and b shows the monthly mean spatial distribution of surface CO and column CO averaged over day and night, for January 2009, i.e. the cruise period. It may be noted that these spatial patterns of surface CO and column CO are more or less similar. The day-to-night changes are marginal, except for slight increase over Indo-Gangetic Plains (north India) during the night (figure not shown). The prominent feature in these figures is the hotspots in CO (both surface mixing ratios and column content) over the East Asian/China region (shown by red/yellow colour) and Bangladesh and eastern Indo-Gangetic Plains (IGP) (orange/yellow). Wang et al. (2001) have reported CO mixing ratios as high as 340 ppbv in July to 808 ppbv in January over East Asian/Chinese region by insitu measurements. Observations by Kar et al. (2008) indicated signature of high CO emissions over Bangladesh and eastern part of an IGP. The spatial variation in CO observed during the present campaign (Fig. 3) was examined in the light of the above spatial maps and airmass back-trajectories obtained using Hybrid Single particle Lagrangian Integrated Trajectory (HYSPLIT) model (Draxler and Rolph, 2003; Rolph, 2003). Five-day back-trajectories arriving at 100 m above ground level (within the boundary layer) at 00, 06, 12 and 18 UT are taken for this analysis (NOAA ARL website http://www.arl.noaa.gov/ready.html). A close examination of the trajectories reveals that trajectory to trajectory variation over a day is very small in terms of their origin and path. In view of the regional/spatial variations of CO mixing ratio over BoB (as seen in Fig. 3b), airmass back-trajectories reaching the cruise track are grouped region wise.

Fig. 11a represents the back-trajectories reaching the ship when it was making measurements over head-BoB. These

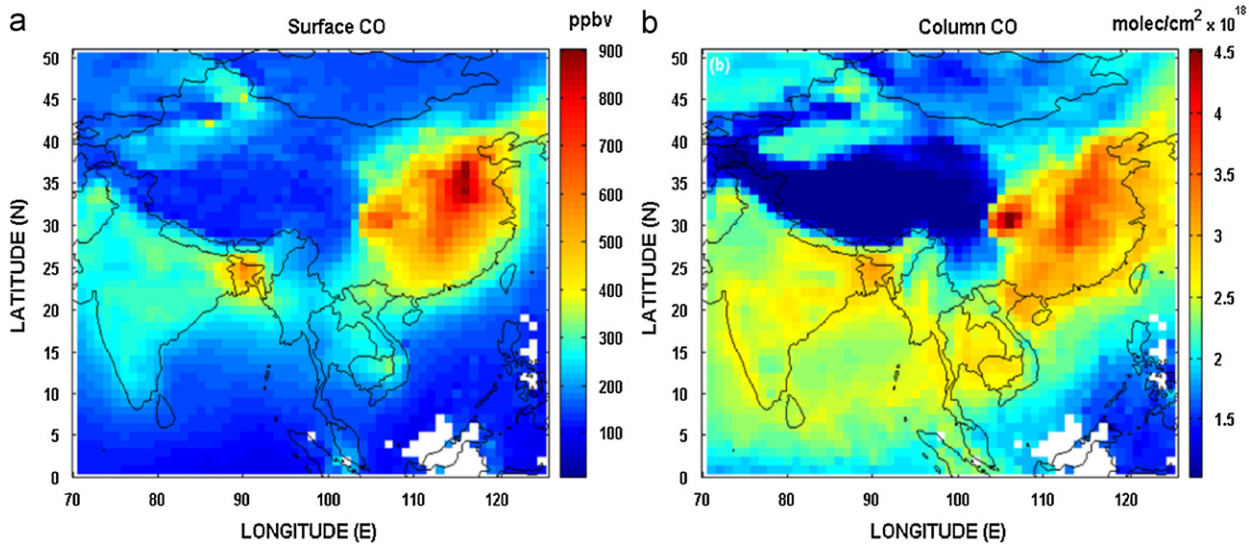

Fig. 10. Month-averaged (a) surface CO mixing ratio (ppbv) and (b) total column CO (molecules/cm^2) obtained from MOPITT level-3 V4 for January 2009. It is the average of day and night retrievals.

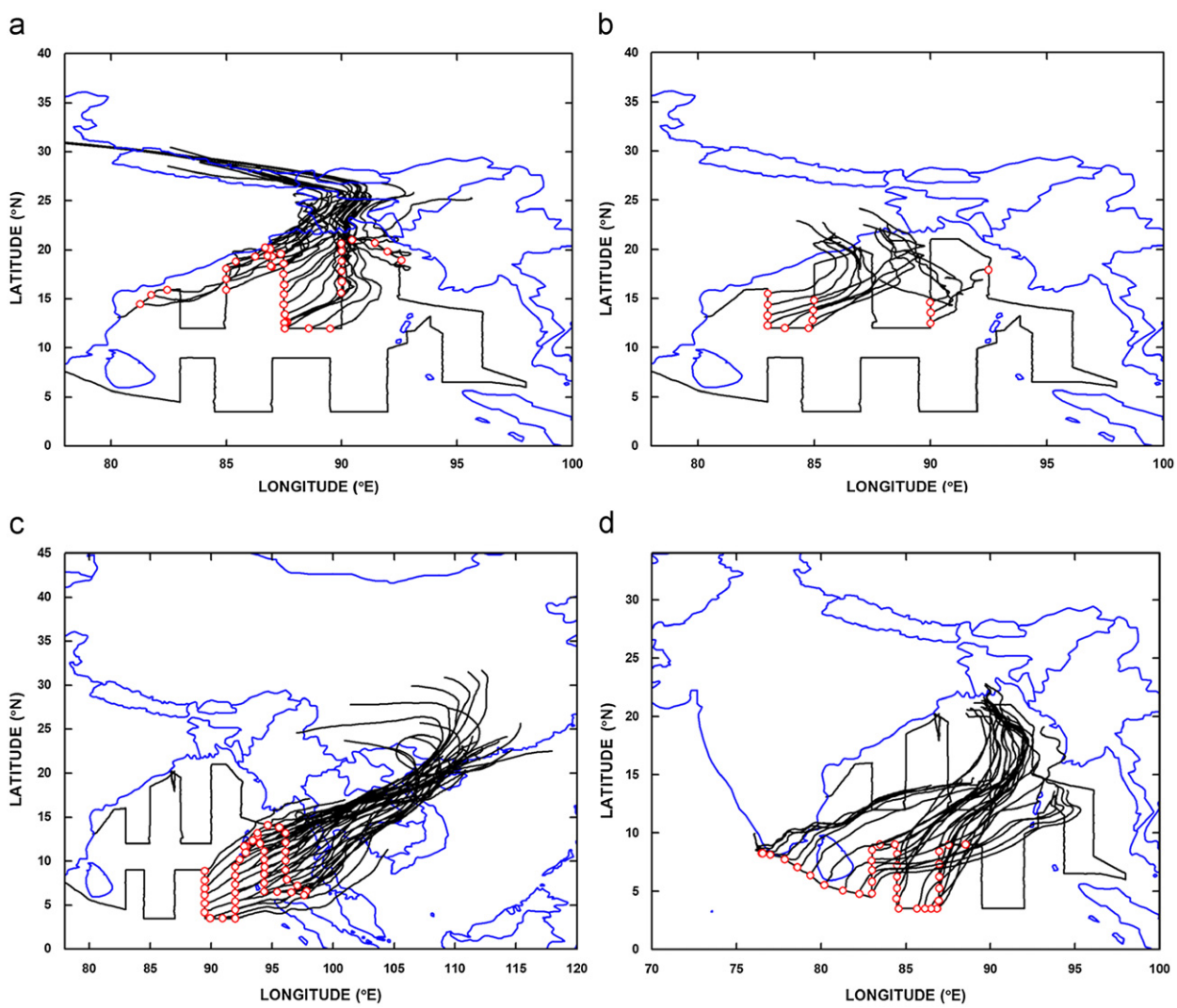

Fig. 11. a–d. Five-day back-trajectories obtained from HYSPLIT model for different locations of the ship during cruise. Circles on cruise track represent the end points of the respective trajectories.

trajectories originate from north/north west landmass and pass through regions north of head-BoB (Bangladesh/WestBengal). Obviously, they originate at regions where surface CO and column CO values are 200–300 ppbv and 1.5×10^{18}–2.5×10^{18} molecules/cm^2, respectively, and pass through a hot spot region, where the surface CO and total CO values are in the range 500–600 ppbv and 3×10^{18}–3.3×10^{18} molecules/cm^2 (in Fig. 10a and b), respectively. The in-situ measured surface CO mixing ratios over head-BoB are comparable or slightly lower than those seen at the location of origin of airmass or enroute. Fig. 11b shows the trajectories reaching the region of 12°–16°N latitude and 83°–85°E and 90°E longitudes, where observed CO mixing ratios are low compared to those over head-BoB. Most of the trajectories reaching this region traverse the Indian landmass, where CO values are low and comparable to those observed over this marine environment (~200–300 ppb). In the region south of 14°N latitude and 89°–98°E longitude (southeast-BoB), highest CO mixing ratio has been observed (upto ~480 ppbv) as can be seen from Fig. 3a. It is interesting to note that most of the trajectories reaching here (Fig. 11c) originate/pass through east-Asian regions/China, where surface as well as column CO values are extremely high (500–900 ppbv and 3×10^{18}–5×10^{18} molecues/cm^2, respectively, as seen in Fig. 10a and b). As per inventory of air pollutant emissions by Streets et al. (2003), in the year 2000, total Asian CO emission was 279 Tg, in which contribution by China was ~116 Tg. However, the surface CO measured over south-east BoB region is low compared to those over the region of origin of airmass. In this context, it is to be noted that, in this region (southeast-BoB), wind-speed is high and within 5-days air parcels travelled more than ~15° in longitude as indicated by the back-trajectories. On the way, the airmass also encountered less polluted regions and got diluted, resulting in lower concentration as compared to concentration at the source region. Similar to the transport from Asian region shown here, de Gouw et al. (2004) has shown transport of several trace gases from a different region of Asia viz. India, Southeast Asia, China, etc. Fig. 11d shows the trajectories reaching the ship when it sailed through south/south-western part of BoB, where CO mixing ratios were low (~167 ± 39 ppbv). These trajectories originate near to the coastal regions of landmasses on the eastern side of head-BoB. As trajectories show, the airmass has travelled long marine path, where there is no strong source of CO, before reaching the ship. Hence, even though the trajectories originate at regions of relatively high CO (head-BoB), lower mixing ratios are observed over south west BoB due to their long path in the marine environment and subsequent dispersion/removal due to favourable wind-speed and direction. In this context, it may also be noted that due to short transit times (5-days), CO loss due to reaction with OH may not be significant. So the differences can reliably be said to be due to dispersion/diffusion.

In order to identify the important geographic source areas contributing to measured concentration, PSCF analysis is widely used (Poirot and Wishinshi, 1986; Poissant, 1999; Lin et al., 2001; Polissar et al., 2001; Begum et al., 2005). PSCF is defined as

$$\mathbf{PSCF} = \frac{m_{ij}}{n_{ij}}$$

where n_{ij} denotes the total number of trajectory segment endpoints falling in the grid cell (i,j) and m_{ij} is the number of times that the source concentration was high (exceeded the arbitrary threshold), when the trajectories passed through the cell (i,j) (Cheng et al., 1993; Pekney et al., 2006). In this case, PSCF indicates the conditional probability that an air parcel passing over the cell (i,j) on its way to the receptor site arrives at the site with concentration values above the threshold (which is taken as > 75% of the maximum value measured in this study). Hence, high values in the spatial distribution of PSCF will pinpoint geographical regions that are likely to produce high concentration values at the receptor site, if crossed by a trajectory.

In the present study, PSCF analysis is carried out for three different regions over cruise track with distinct CO mixing ratio pattern, using *TrajStat* software (http://ready.arl.noaa.gov/HYSPLIT.php). They include southeast-BoB, where highest CO values were observed, head-BoB with slightly lower values and for southwest-BoB where lowest CO mixing ratios were observed. Seven-day airmass back-trajectories and the measured CO values in these regions formed the input information to identify possible transport pathways and source areas. Generally, PSCF analysis is done with region representative stationary point measurements. But in this study, since the measurement platform is moving, the data collected are both spatially and temporally separated. This puts a limitation in using the cruise data. Hence, the analysis was conducted using the satellite measured CO values available on day-to-day basis for each location. Daily averaged CO mixing ratio for 7 days, in each region, obtained from MOPITT measurements, along with 7-day airmass back-trajectories are used in the calculation of PSCF. Fig. 12a–c shows the contribution from different source regions to head-BoB, Southeast-BoB and south-west-BoB, respectively. The groups of 7days back-trajectories are also shown in Fig. 2. The contribution to head-BoB is a very high from nearby region and from Bangladesh region, as seen from Fig. 12a. On the other hand, source regions for high CO over southeast-BoB are distributed along the trajectory path (Fig. 12b), and there is a significant contribution from east-Asian region.

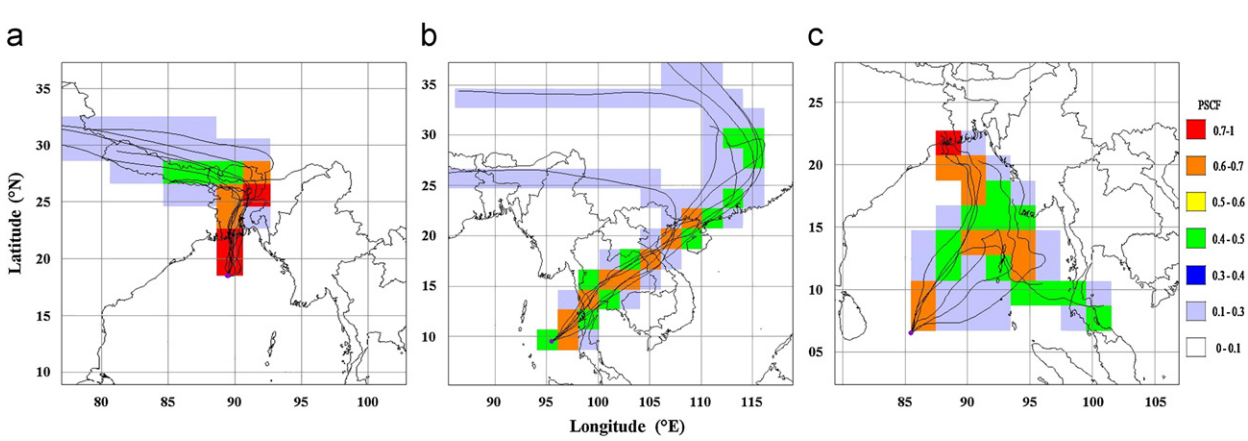

Fig. 12. PSCF analysis for (a) head-BoB, (b) southeast-BoB and (c) southwest-BoB during the period, where ship was taking measurements over the respective region. The lines represent back-trajectories.

Table 2
Comparison of CO mixing ratios measured over BoB in different seasons as measured during various campaigns.

Experiment/campaign and reference	Period of study	CO mixing ratio	
		Head-BoB (north of 16°N)	Southwest-BoB (south of 16°N,west of 87°E)
INDOEX (Mühle et al. 2002)	February–March 1999	No data	100–170 ppbv
BOBEX (Lal et al., 2006)	February–March 2001	150–275 ppbv	100–350 ppbv
BOBPS (Sahu et al., 2006)	September–October 2002	108–180 ppbv	108–210 ppbv (most of the values are below 180 ppbv)
W_ICARB (Present study)	December 2008–January 2009	290 ± 72 ppbv (140–460 ppbv)	167 ± 39 ppbv (80–300 ppbv)

PSCF distribution over south-west BoB shows a different picture with the significant contribution from the surrounding grids. Even though, head-BoB and southeast-BoB contributed to this region (see the high PSCF grids), the CO mixing ratios are relatively low, probably due to the long marine path encountered.

5.4. Comparison with earlier measurements

Earlier studies on CO over BoB are also based on campaign mode observations conducted during INDOEX, BOBEX and BOBPS (Mühle et al. 2002; Lal et al., 2006; Sahu et al., 2006). While INDOEX was conducted during February–March (winter to spring transition period) 1999; BOBEX was conducted during same months, but in 2001, and BOBPS was during post-monsoon months of September–October 2002. The present study has brought out the wintertime pattern of CO over BoB. Furthermore, this study is more extensive in terms of latitudinal and longitudinal coverage. For the first time, measurements were carried out over the eastern BoB region which was unexplored in earlier campaigns. However, all these cruises covered common regions like head-BoB and south-west BoB, except INDOEX, during which measurements were not available over head-BoB. Table 2 gives a comparison of CO mixing ratio corresponding to the common area covered by different cruises. Obviously, the CO mixing ratio is highest during winter months of December–January (i.e. the present cruise) compared to premonsoon/post-monsoon period. Also, the seasonal variation in CO mixing ratio is more significant over head-BoB compared to south west BoB. During all these seasons, spatial pattern of CO mixing ratio is found to be influenced by advection from continental landmass (Mühle et al. 2002; Lal et al., 2006; Sahu et al., 2006). The present study also has brought out an evidence of strong transport of pollutants over to south-eastern BoB in winter from China and other eastern Asian countries.

6. Summary

Results of the present study on near-surface-CO over BoB during winter (December 2008–January 2009) along with the synoptic wind pattern obtained from NCEP/NCAR reanalysis, airmass back-trajectories from HYSPLIT model and MOPITT-retrieved CO can be summarized as follows.

- Mixing ratio of CO over BoB exhibits large spatial variation with high values of the order of 290 ± 72 over head-BoB, 379 ± 58 ppbv over southeast-BoB and low values of 167 ± 39 ppbv over southwest-BoB. In addition to transport, regional emission distribution also plays a crucial role in establishing this pattern.
- Based on the HYSPLIT back-trajectory analysis and satellite retrieved spatial map of CO in the Asian region, different pathways of transport have been identified. While transport from northern landmass caused high levels of CO over head-BoB, that from east-Asia/Chinese landmass is responsible for the enhanced CO levels over eastern BoB.
- PSCF analysis shows that, for head-BoB, source region is focused over Bangladesh and for southeast-BoB, source is distributed over China and other eastern Asian countries.
- Comparison of the in-situ measured surface data with satellite-based data from MOPITT (level-3 V4) shows good agreement, except the region of southeast-BoB where highest CO mixing ratios were observed.
- The mixing ratio of CO measured during December–January (winter) are higher over head-BoB and comparable over southwest-BoB to those measured during other campaigns conducted in February–March 1999, 2001 and September–October, 2002.

Acknowledgements

MOPITT level-3 data used in this study were obtained from the NASA Langley Research Center Atmospheric Sciences Data Center. The authors gratefully acknowledge the NOAA Air Resources Laboratory (ARL) for the provision of the HYSPLIT transport and dispersion model and/or READY website (http://www.arl.noaa.gov/ready.php) used in this publication. Winds are obtained from NCEP Reanalysis data provided by the NOAA/OAR/ESRL PSD, Boulder, Colorado, USA, from their website at http://www.esrl.noaa.gov/psd/. The authors acknowledge Dr. D. Bala Subrahamanyam and Dr. N. V. P. Kiran Kumar for providing meteorological data recorded onboard ship. The authors gratefully acknowledge Dr. C. B. S. Dutt, Deputy Programme Director, ISRO-GBP for kind support and encouragement.

References

Asnani, G.C., 1993. Trop. Meteorol.. Indian Institute of Tropical Meteorology, Pashan, Pune, India.
Begum, B.A., Kim, E., Jeong, C., Lee, D., Hopke, P.K., 2005. Evaluation of the potential source contribution function using the 2002 Quebec forest fire episode. Atmos. Environ. 39, 3719–3724.
Brühl, C., Crutzen, P.J., 1999. Reductions in the anthropogenic emissions of CO and their effect on CH_4. Chemosphere: Global Change Sci. 1, 249–254.
Cheng, M.-D., Hopke, P.K., Zeng, Y., 1993. A receptor-oriented methodology for determining source regions of particulate sulfate at Dorset, Ontario. J. Geophys. Res. 98, 16839–16849.
Crutzen, P.J., Andreae, M.O., 1990. Biomass burning in the tropics: impact on atmospheric chemistry and biogeochemical cycles. Science 250 (4988), 1669–1678.
Dianov-Klokov, V.I., Yurganov, L.N., 1989. Spectroscopic measurements of atmospheric carbon monoxide and methane. 2: Seasonal variations and long-term trends. J. Atmos. Chem. 8, 153–164.
Draxler, R.R., Rolph, G.D., 2003. HYSPLIT (HYbrid Single-Particle Lagrangian Integrated Trajectory) Model access via NOAA ARL READY Website (http://www.arl.noaa.gov/HYSPLIT.php). NOAA Air Resources Laboratory, Silver Spring, MD.
Edwards, D.P., Edwards, D.P., Lamarque, J.-F., Attié, J.-L., Emmons, L.K., Richter, A., Cammas, J.-P., Gille, J.C., Francis, G.L., Deeter, M.N., Warner, J., Ziskin, D.C., Lyjak, L.V., Drummond, J.R., Burrows, J.P., 2003. Tropospheric ozone over the tropical Atlantic: a satellite perspective. J. Geophys. Res. 108 (D8), 4237.
Edwards, D.P., Emmons, L.K., Gille, J.C., Chu, A., Attié, J.-L., Giglio, L., Wood, S.W., Haywood, J., Deeter, M.N., Massie, S.T., Ziskin, D.C., Drummond, J.R., 2006.

Satellite-observed pollution from Southern Hemisphere biomass burning. J. Geophys. Res. 111, D14312.
Eisinger, D., Dougherty, S.K., Chang, D., Kear, T., Morgan, P., 2002. A Reevaluation of Carbon Monoxide: past Trends, Future Concentrations, and Implications for Conformity 'Hot Spot' Policies. J. Air Waste Manage. Assoc. 52 (9), 1012–1025.
Fisher, R.A., 1970. Statistical Methods for Research Workers fourteenth ed. Oliver and Boyd, Edinburgh 362 pp.
Granier, C., Petron, G., Müller, J., Brasseur, G., 2000. The impact of natural and anthropogenic hydrocarbons on the tropospheric budget of carbon monoxide. Atmos. Environ. 34, 5255–5270.
Grechko, E.I., Dzhola, A.V., Golitsyn, G.S., 2000. Variations of carbon monoxide, ethane, and water vaporin the total atmospheric column over Russia (Zvenigorod station) between 1970 and 1999. In: Tenth ARM Science Team Meeting Proceedings, San Antonio, Texas, March 13–17, 2000.
Heald, C.L., Jacob, D.J., Fiore, A.M., Emmons, L.K., Gille, J.C., Deeter, M.N., Warner, J., Edwards, D.P., Crawford, J.H., Hamlin, A.J., Sachse, G.W., Browell, E.V., Avery, M.A., Vay, S.A., Westberg, D.J., Blake, D.R., Singh, H.B., Sandholm, S.T., Talbot, R.W., Fuelberg, H.E., 2003. Asian outflow and transpacific transport of carbon monoxide and ozone pollution: an integrated satellite, aircraft and model perspective. J. Geophys. Res. 108 (D24), 4804.
Holloway, T., Levy, H., Kasibhatla, P., 2000. Global distribution of carbon monoxide. J. Geophys. Res. 105, 12123–12147.
Jones, R., Amador, J., 1993. Methane and carbon monoxide production, oxidation, and turnover times in the Caribbean Sea as influenced by the Orinoco River. J. Geophys. Res. 98 (C2), 2353–2359.
Kar, J., Bremer, H., Drummond, J.R., Rochon, Y.J., Jones, D.B.A., Nichitiu, F., Zou, J., Liu, J., Gille, J.C., Edwards, D.P., Deeter, M.N., Francis, G., Ziskin, D., Warner, J., 2004. Evidence of vertical transport of carbon monoxide from measurements of pollution in the troposphere (MOPITT). Geophys. Res. Lett. 31, L23105.
Kar, J., Drummond, J.R., Jones, D.B.A., Liu, J., Nichitiu, F., Zou, J., Gille, J.C., Edwards, D.P., Deeter, M.N., 2006. Carbon monoxide (CO) maximum over the Zagros mountains in the Middle East: signature of mountain venting? Geophys. Res. Lett. 33 L15819.
Kar, J., Jones, D.B.A., Drummond, J.R., Attié, J.L., Liu, J., Zou, J., Nichitiu, F., Seymour, M.D., Edwards, D.P., Deeter, M.N., Gille, J.C., Richter, A., 2008. Measurement of low-altitude CO over the Indian subcontinent by MOPITT. J. Geophys. Res. 113, D16307.
Khalil, M.A.K., Rasmussen, R.A., 1988. Carbon monoxide in the Earth's atmosphere: indications of a global increase. Nature 332, 242–245.
Khalil, M.A.K., Rasmussen, R.A., 1994. Global decrease in atmospheric carbon monoxide concentration. Nature 370, 639–641.
Klonecki, A., Levy II, H., 1997. Tropospheric chemical ozone tendencies in $CO–CH_4–NO_y–H_2O$ system: their sensitivity to variations in environmental parameters and their application to a global chemistry transport model study. J. Geophys. Res. 102 (D17), 21221–21237.
Langenfelds, R.L., Francey, R.J., Pak, B.C., Steele, L.P., Lloyd, J., Trudinger, C.M., Allison, C.E., 2002. Interannual growth rate variations of atmospheric CO_2 and its delta ^{13}C, H_2, CH_4, and CO between 1992 and 1999 linked to biomass burning. Global Biogeochem. Cycles 16 (3), 21-1–21-22.
Lal, S., Chand, D., Sahu, L.K., Venkataramani, S., Brasseur, G., Schultz, M.G., 2006. High levels of ozone and related gases over the Bay of Bengal during winter and early spring of 2001. Atmos. Environ. 40, 1633–1644.
Li, C., Marufu, L.T., Dickerson, R.R., Li, Z., Wen, T., Wang, Y., Wang, P., Chen, H., Stehr, J.W., 2007. In situ measurements of trace gases and aerosol optical properties at a rural site in northern China during East Asian study of Tropospheric Aerosols: an international regional experiment 2005. J. Geophys. Res. 112 (D22S04).
Li, Q., Jacob, D.J., Park, R., Wang, Y., Heald, C.L., Hudman, R., Yantosca, R.M., Martin, R.V., Evans, M., 2005. North American pollution outflow and the trapping of convectively lifted pollution by upper-level anticyclone. J. Geophys. Res. 110, D10301.
Lin, C.-J., Cheng, M.-D., Schroeder, W.H., 2001. Transport patterns and potential sources of total gaseous mercury measured in Canadian high Arctic in 1995. Atmos. Environ. 35 (6), 1141–1154.
Liu, J., Drummond, J.R., Li, Q., Gille, J.C., Ziskin, D.C., 2005. Satellite mapping of CO emission from forest fires in northwest America using MOPITT measurements. Remote Sensing. Environ. 95, 502–516.
Liu, J., Drummond, J.R., Jones, D.B.A., Cao, Z., Bremer, H., Kar, J., Zou, J., Nichitiu, F., Gille, J.C., 2006. Large horizontal gradients in atmospheric CO at the synoptic scale as seen by spaceborne measurements of pollution in the troposphere. J. Geophys. Res. 111, D02306.
Logan, J.A., Prather, M.J., Wofsy, S.C., McElroy, M.B., 1981. Tropospheric chemistry—a global perspective. J. Geophys. Res. 86, 7210–7254.
Mühle, J., Zahn, A., Brenninkmeijer, C.A.M., Gros, V., Crutzen, P.J., 2002. Air mass classification during the INDOEX R/V cruise using measurements of non-methane hydrocarbons, CH, CO_2, CO, ^{14}CO, and $\delta^{18}O(CO)$. J. Geophys. Res. 107 (D19), 8021.
Novelli, P.C., Steele, L.P., Tans, P.P., 1992. Mixing ratios of carbon monoxide in the troposphere. J. Geophys. Res. 97, 20 731–20 750.
Ohta, K., 1997. Diurnal variation of carbon monoxide concentration in the Equatorial Pacific upwelling region. J. Oceanogr. 53, 173–178.
Pekney, N.J., Davidson, C.,.I., Zhou, Liming, Hopke, Philip K., 2006. Application of PSCF and CPF to PMF-modeled sources of PM2.5 in Pittsburgh. Aerosol Sci. Technol. 40 (10), 952–961.
Poirot, R.L., Wishinshi, P.R., 1986. Visibility, sulfate, and air mass history associated with the summertime aerosol in northern Vermont. Atmos. Environ. 20, 1457–1469.
Poissant, L., 1999. Potential sources of atmospheric total gaseous mercury in the St. Lawrence river valley. Atmos. Environ. 33, 2537–2547.
Polissar, A.V., Hopke, P.K., Harris, J.M., 2001. Source regions for atmospheric aerosol measured at Barrow, Alaska. Environ. Sci. Technol. 35, 4214–4226.
Rolph, G.D. (2003). Real-time Environmental Applications and Display sYstem (READY) Website (http://www.arl.noaa.gov/ready.php). NOAA Air Resources Laboratory, Silver Spring, MD.
Sahu, L.K., Lal, S., Venkataramani, S., 2006. Distribution of O_3, CO and hydrocarbons over Bay of Bengal: a study to assess the role of transport from southern India and marine regions during September–October 2002. Atmos. Environ. 40, 4633–4645.
Steele, L.P., Krummel, P.B., Langenfelds., R.L., 2003. Atmospheric CO concentrations from sites in the CSIRO Atmospheric Research GASLAB air sampling network (October 2002 version). In: Trends, A. (Ed.), Compendium of Data on Global Change. Carbon Dioxide Information Analysis Center, Oak Ridge National Laboratory, U.S. Department of Energy, Oak Ridge, TN, U.S.A.
Streets, D.G., Bond, T.C., Carmichael, G.R., Fernandes, S.D., Fu, Q., He, D., Klimont, Z., Nelson, S.M., Tsai, N.Y., Wang, M.Q., Woo, J.-H., Yarber, K.F., 2003. An inventory of gaseous and primary aerosol emissions in Asia in the year 2000. J. Geophys. Res. 108 (D21), 8809.
Stubbins, A.P., Uher, G., Law, C.S., Mopper, K., Robinson, C., Upstill-Goddard, R.C., 2006. Open-ocean carbon monoxide photoproduction. Deep-Sea Res. II 53, 1695–1705.
Swinnerton, J.W., Linnenbom, V.J., LaMontagne, R.A., 1970. The ocean: a natural source of carbon monoxide. Science 167, 984–986.
Thompson, A.M., 1992. The oxidizing capacity of the Earth's atmosphere: probable past and future changes. Science 256, 1157–1165.
Wang, C., Prinn, R.G., 1999. Impact of emissions, chemistry, and climate on atmospheric carbon monoxide: 100-year predictions from a global chemistry-climate model. Chemosphere—Global Change Sci. 1, 73–82.
Wang, T., Cheung, V.T.F., Anson, M., Li, Y.S., 2001. Ozone and related gaseous pollutants in the boundary layer of eastern China: overview of the recent measurements at a rural site. Geophys. Res. Lett. 28 (12), 2373–2376.
Zander, R., DemoulinPh., R., Ehhalt, D.H., Schmidt, U., Rinsland, C.P., 1989. Secular increase of the total vertical column abundance of carbon monoxide above central Europe since 1950. J. Geophys. Res. 94 (D8), 11,021–11,028.
Zhang, R., Wang, M., Ren, L., 2001. Long-term trends of carbon monoxide inferred using a two-dimentional model. Chemosphere—Global Change Sci. 3, 123–132.
Zuo, Y., Guerrero, M.A., Jones, A.D., 1998. Reassessment of the ocean-to-atmosphere flux of carbon monoxide. Chem. Ecol. 14, 241–257.
de Gouw, J.A., Cooper, O.R., Warneke, C., Hudson, P.K., Fehsenfeld, F.C., Holloway, J.S., Hübler, G., Nicks Jr., D.K., Nowak, J.B., Parrish, D.D., Ryerson, T.B., Atlas, E.L., Donnelly, S.G., Schauffler, S.M., Stroud, V., Johnson, K., Carmichael, G.R., Streets, D.G., 2004. Chemical composition of air masses transported from Asia to the U.S. West Coast during ITCT 2K2: fossil fuel combustion versus biomass-burning signatures. J. Geophys. Res. 109 (D23S20).